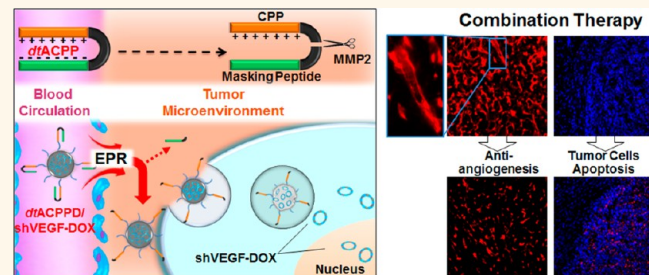


Tumor-Targeting and Microenvironment-Responsive Smart Nanoparticles for Combination Therapy of Antiangiogenesis and Apoptosis

Shixian Huang, Kun Shao, Yang Liu, Yuyang Kuang, Jianfeng Li, Sai An, Yubo Guo, Haojun Ma, and Chen Jiang*

Key Laboratory of Smart Drug Delivery, Ministry of Education & PLA, Department of Pharmaceutics, School of Pharmacy, Fudan University, Shanghai 201203, China

ABSTRACT Tumor microenvironment, such as the lowered tumor extracellular pH (pHe) and matrix metalloproteinase 2 (MMP2), has been extensively explored, which promotes the development of the microenvironment-responsive drug delivery system. Utilizing these unique features, an activatable cell-penetrating peptide (designated as *dtACPP*) that is dual-triggered by the lowered pHe and MMP2 has been constructed, and a smart nanoparticle system decorating with *dtACPP* has been successfully developed, which could dual-load gene drug and chemotherapeutics simultaneously. After systemic administration, *dtACPP*-modified nanoparticles possess passive tumor targetability *via* the enhanced permeability and retention effect. Then *dtACPP* would be activated to expose cell-penetrating peptide to drive the nanoparticles' internalization into the intratumoral cells. As angiogenesis and tumor cells might be mutually improved in tumor growth, so combining antiangiogenesis and apoptosis is meaningful for oncotherapy. Vascular endothelial growth factor (VEGF) is significant in angiogenesis, and anti-VEGF therapy could decrease blood vessel density and delay tumor growth obviously. Chemotherapy using doxorubicin (DOX) could kill off tumor cells efficiently. Here, utilizing *dtACPP*-modified nanoparticles to co-deliver plasmid expressing interfering RNA targeting VEGF (shVEGF) and DOX (designated as *dtACPPD/shVEGF-DOX*) results in effective shutdown of blood vessels and cell apoptosis within the tumor. On the premise of effective drug delivery, *dtACPPD/shVEGF-DOX* has demonstrated good tumor targetability, little side effects after systemic administration, and ideal antitumor efficacy.



KEYWORDS: cell-penetrating peptide · chemotherapy · combination therapy · tumor microenvironment · tumor-targeting nanoparticles · VEGF

Both angiogenesis and proliferation of tumor cells are the main features of tumor tissues.^{1,2} To progress and satisfy the proliferating tumor cells for nutrients and oxygen, the tumors stimulate the formation of new blood vessels through processes driven primarily by vascular endothelial growth factor (VEGF).^{2–4} Meanwhile, VEGF is overexpressed and secreted mostly by tumor cells, which could stimulate proliferation of endothelial cells, causing angiogenesis in tumor tissue.^{5,6} As angiogenesis and tumor cells might be mutually improved, it is necessary and practical to carry out the dual therapy, meaning antiangiogenesis and killing off tumor cells simultaneously.⁶

Most patients with advanced tumor encounter cancer-associated systemic syndrome (CASS), which is generally well correlated with the level of circulating VEGF and significantly impairs the quality of life and shortens lifespan.⁷ Regarding the significant role of VEGF in angiogenesis and tumor progression, many clinical trials targeting VEGF-signaling pathways are under development,^{8,9} and the first anti-VEGF agent, humanized monoclonal antibody, Bevacizumab, has been approved for use in patients with cancer.¹⁰

RNA interference (RNAi), a promising technique in oncotherapy, can selectively inhibit target gene expression and improve the sensitivity of chemotherapeutics.^{11,12}

* Address correspondence to jiangchen@shmu.edu.cn.

Received for review February 1, 2013 and accepted March 1, 2013.

Published online March 01, 2013
10.1021/nn400548g

© 2013 American Chemical Society

RNAi-mediated silencing VEGF expression has been proven to inhibit the expression of VEGF successfully, resulting in decreased blood vessel density and delayed tumor growth.^{13–15} Anti-VEGF agent alone might be not sufficient to cause complete inhibition of tumor growth but could increase the penetration of co-medication into tumors by reducing the intratumoral pressure and normalizing abnormal and non-functional capillary networks.¹⁶ In order to achieve ideal antitumor efficacy, it is necessary to combine chemotherapeutics with anti-VEGF agent,¹⁰ and doxorubicin (DOX) is widely used and could efficiently kill off tumor cells.

The anti-VEGF agent used in this study was shVEGF. For the combination therapy of gene and chemotherapeutics, co-delivery is necessary to avoid the multiple dosing or respective constructions of the delivery system.¹⁷ Inspiringly, DOX could intercalate into a double helix of DNA to form a plasmid–DOX complex, shVEGF–DOX, with the presence of the flat aromatic ring, a process requiring no modification of shVEGF or DOX.^{18,19} Such intercalation can protect the plasmid against nucleases and improve pharmacokinetics of DOX by increasing blood circulation in return.¹⁸ Hence, it would favor the expression of shVEGF to inhibit VEGF; meanwhile, DOX could kill off tumor cells more effectively. In light of these advantages, shVEGF–DOX complex might make co-delivery and combination therapy easier to implement.^{20,21}

It is noteworthy that angiogenesis is also a physiological process in some organs and constitutes a normal response to injury.^{22,23} Meanwhile, the non-specific distribution of DOX throughout the whole body introduces systemic toxicity and limits effective treatment.²⁴ So for systemic administration, it is significant to selectively deliver shVEGF–DOX to the tumor site, which is not only the premise of therapeutic effect but also free of systemic antiangiogenesis and toxicity to reduce side effects.

Tumor-targeting nanoparticles tend to accumulate in the tumors by the prolonged circulation and enhanced permeability and retention (EPR) effect.^{25–27} Then, nanoparticles require cellular internalization for therapeutic outcome. Cell-penetrating peptide (CPP) has been researched extensively for the efficient cell internalization, while the *in vivo* application is a nightmare as CPP lacks selectivity.^{28–30} In order to overcome this *in vivo* bottleneck, it is necessary and feasible to quench the cell-penetrating property of CPP in the circulation and recover its intrinsic characteristics within the tumor.^{31,32} Here, an activatable CPP (*dt*ACPP) dual-triggered by the unique tumor microenvironment, lowered pH_e (pH 5.8–7.2), and upregulated MMP2 was constructed.^{31–34} In *dt*ACPP, the internalization function of polycationic CPP was quenched by a covalently attached pH-sensitive masking peptide, linking by a MMP2 substrate. In the circulation,

the masking peptide (electric point about 6.4) would be negatively charged to shield CPP well, while this shielding effect would be eliminated within the tumor. Accompanying the cleavage of linker by MMP2, *dt*ACPP would be activated to CPP. Hence, CPP that recovered to the state of freedom would internalize the nanoparticles merely into the intratumoral cells.

Of the nonviral vector, dendrigrift poly-L-lysine (DGL) is widely investigated for gene delivery to the tumor because of its ability to effectively complex and condense DNA to form nanoparticles.^{35,36} As shown in Scheme 1, *dt*ACPP was conjugated to the surface of DGL via α -maleimidyl- ω -N-hydroxysuccinimidyl polyethyleneglycol (MAL-PEG-NHS) to construct the gene nanocarrier, *dt*ACPP-PEG-DGL (*dt*ACPPD). Condensed nanoparticles, *dt*ACPPD/shVEGF–DOX, were formed through electrostatic interactions between cationic DGL and negatively charged plasmid shVEGF. The tumor-targeting nanoparticles were endowed with steric stabilization to perform the EPR effect well and enhanced internalization to deliver shVEGF–DOX into the intratumoral cells efficiently. In this case, antiangiogenesis and apoptosis of tumor cells occurred simultaneously.

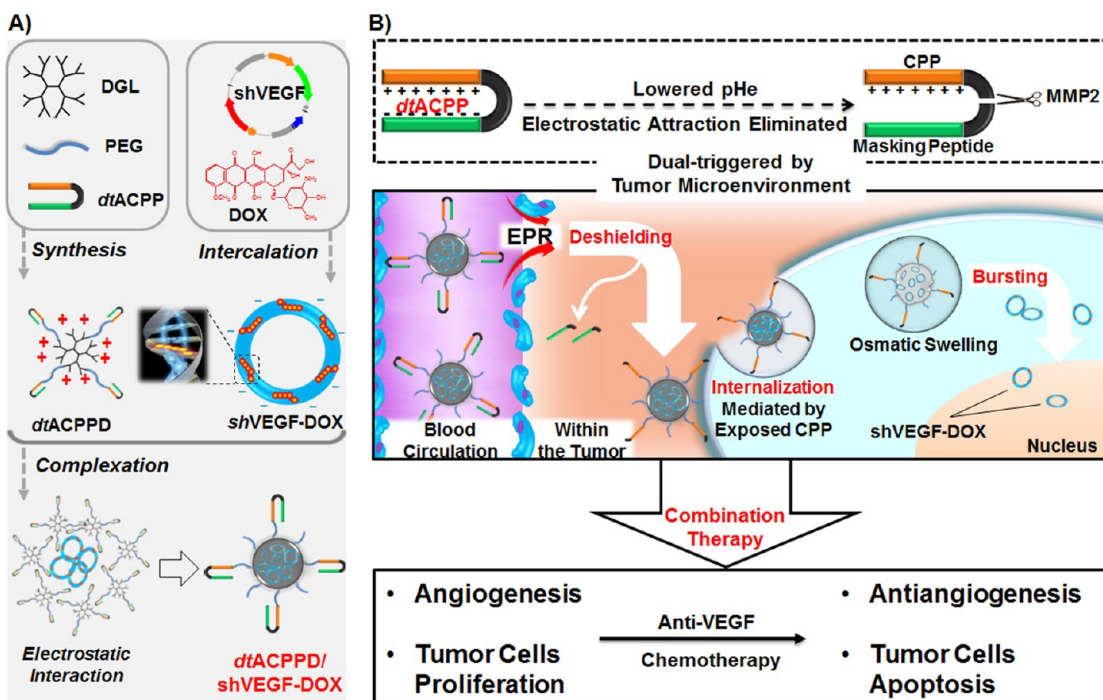
Glioma is the one of the most aggressive malignant tumors and is nearly always fatal.³⁷ Clinically, despite therapy, 6 month progression-free survival for relapsed or progressive glioma is 9–21%, and median overall survival is 30 weeks or less.³⁸ In this study, the glioma-bearing mice were constructed to systematically evaluate the mechanism and corresponding therapeutic efficacy of *dt*ACPPD/shVEGF–DOX both *in vitro* and *in vivo*.

RESULTS AND DISCUSSION

Incorporating stimulus-responsive moieties into the targeting drug delivery systems could achieve precise targetability and enhanced cellular internalization.^{31–34} Based on the unique tumor microenvironment, lowered pH_e, and upregulated MMP2, an activatable CPP, *dt*ACPP, was designed for the tumor-targeting delivery of nanoparticles. Here, the extracellular MMP2 and lowered pH_e were utilized as dual stimuli to trigger the enhanced tumor targeting and cellular internalization in our designed nanoparticle system, *dt*ACPPD/shVEGF–DOX.

As angiogenesis and tumor cells might be mutually improved in tumor growth, antiangiogenesis and killing off tumor cells simultaneously might be meaningful for antitumor treatment.⁶ In this study, combining anti-VEGF agent (shVEGF) with chemotherapeutics (DOX) efficiently decreased blood vessels and killed off cells within the tumor, which has achieved ideal antitumor efficacy.

Development of Nanocarriers and Nanoparticles. Cationic polymer nonviral vectors have gained increasing attention because of flexibility in their synthesis and



Scheme 1. (A) Construction of tumor-targeting nanoparticle system, *dtACPPD/shVEGF*–DOX. (B) Tumor-targeting, internalization, and combination therapy strategy of *dtACPPD/shVEGF*–DOX.

structural modifications for specific biomedical application. *dtACPPD* was constructed according to Scheme 1A and further verified by ^1H NMR (Figure 1A). The solvent peak of D_2O was found at $\delta = 4.8$ ppm. The branching units of DGL had multiple peaks between 1.2 and 4.5 ppm. Comparing *dtACPPD* spectrum to PEG-DGL, the characteristic ^1H NMR peak of PEG's repeat units ($-\text{O}-\text{CH}_2-\text{CH}_2-\text{O}-$) at $\delta = 3.6$ ppm still presented, while PEG's MAL at $\delta = 6.8$ ppm (peak I) disappeared and *dtACPPD*'s methyl at $\delta = 0.8$ ppm (peak II) presented. All of the results verified that the MAL group of PEG had reacted with the thiol group of *dtACPPD* and further indicated the successful construction of *dtACPPD*.

The shVEGF–DOX complex was monitored by fluorescence scanning technology because DOX intercalated into shVEGF showed fluorescence quenching. For free DOX, the spectra showed strong fluorescence signal in the range of 520–680 nm (Figure 1B). With the concentration of shVEGF increasing, the signal intensity gradually decreased. DOX totally intercalated into shVEGF at a molar ratio of 3:3000 (shVEGF/DOX), meaning that 0.17 μg of DOX could intercalate completely into 1 μg of shVEGF. In this study, the shVEGF–DOX complex adopted the ratio of 1:0.16 (shVEGF/DOX, w/w).

A fundamental requirement for effective targeting delivery is that the nanocarrier must be able to efficiently complex with therapeutic drugs. The ability of *dtACPPD* to condense shVEGF–DOX at varying weight ratios (DGL/shVEGF, w/w) was evaluated (Figure 1C). In this gel retardation assay, shVEGF–DOX bound to

dtACPPD remained in the loading wells, while the unbound migrated. When the ratio was 6:1, DNA was completely protected from ethidium bromide, showing no staining in the loading well. Protecting DNA from agents such as nucleases is critical to ensure the transfection efficiency. Meanwhile, the electrophoretic mobility of shVEGF–DOX was slower than shVEGF, verifying that DOX intercalated into shVEGF well. In this study, *dtACPPD/shVEGF*–DOX adopted the ratio of 6:1 (DGL/shVEGF, w/w).

dtACPPD/shVEGF–DOX had a unimodal distribution, and the hydrodynamic sizes was 144.9 ± 2.5 nm under pH 7.4 (Figure 1D, left) and 151.8 ± 2.9 nm under pH 6.0 (Figure 1D, right). This size range was suitable for the prolonged blood circulation to perform the EPR effect well.^{29,30} The corresponding zeta-potential values were 1.8 ± 4.1 and 3.5 ± 2.9 mV, respectively. The nanoparticles appeared to be a kind of analogous spherical shape and compacted structure under pH 7.4 and 6.0 (Figure 1E).

Cytotoxicity, Cellular Uptake Studies, and *In Vivo* Targetability. The commonly studied grade IV glioma cell line, U-87 malignant glioma (MG) cells, was chosen for this study because this cell line expresses high levels of VEGF mRNA and protein.^{39,40} In addition, U-87 MG cells are able to form tumors in mice, which favors the construction of the clinically relevant intracranial glioblastoma (GBM) xenograft model, glioma-bearing mice.³⁹

Cytotoxicity is a primary concern in the development of the drug delivery system. Under pH 7.4 or 6.0, *dtACPPD/DNA* (pGL2) showed minimal toxic effect

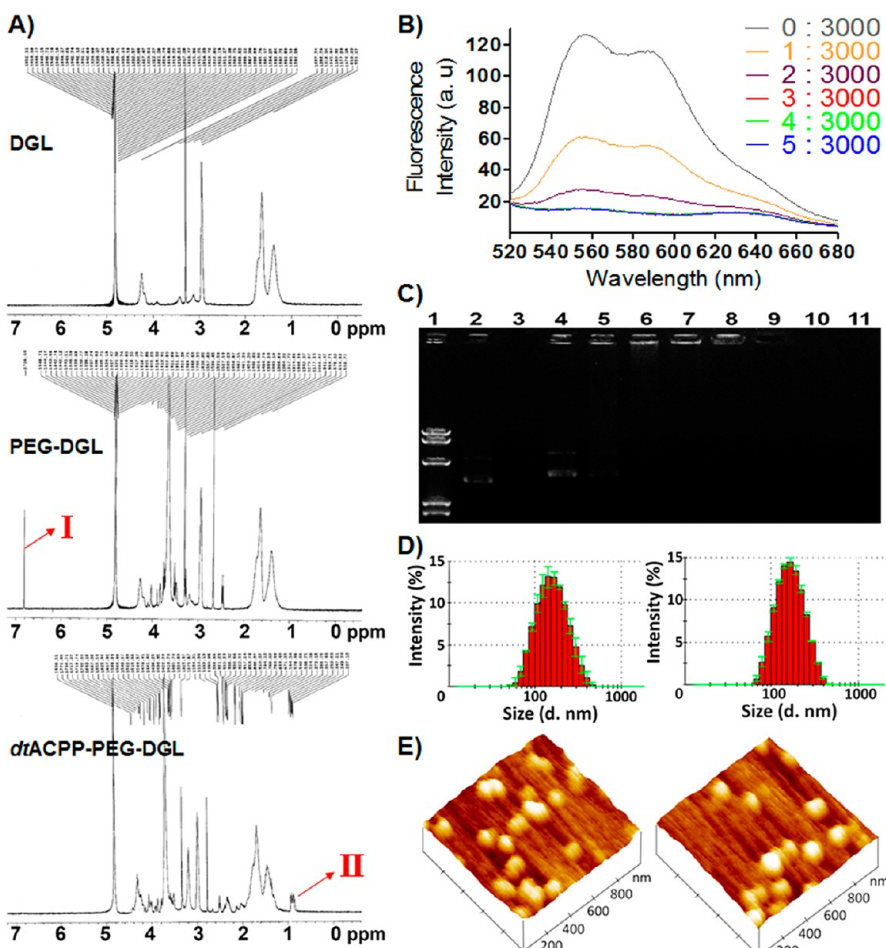


Figure 1. (A) ^1H NMR spectrum of DGL, PEG-DGL, and *dtACPPD* (*dtACPPD*). (B) Fluorescence spectra of DOX solution ($3 \mu\text{M}$) with increasing molar ratios of DNA (from top to bottom, 0:3000, 1:3000, 2:3000, 3:3000, 4:3000, 5:3000 pmol/pmol). (C) Electrophoretic analysis of DNA–DOX binding by *dtACPPD*, in which lane numbers correspond to nanoparticles with different weight ratios (DGL to DNA): (1) DNA marker, (2) naked DNA, (4) DNA–DOX, (5) 0.1:1, (6) 0.5:1, (7) 1:1, (8) 2:1, (9) 4:1, (10) 6:1, (11) 8:1. The particle size distribution of *dtACPPD*/DNA–DOX was analyzed by (D) dynamic light scattering (DLS) zetasizer and (E) atomic force microscope (AFM) under pH 7.4 (left) or pH 6.0 (right).

(Figure 2A). Although the cytotoxicity under pH 6.0 was slightly increased, the cell viability was still more than 90% at $50 \mu\text{g}$ of DGL/mL, the concentration that was adopted in the following *in vitro* study, confirming that *dtACPPD* was a secure platform for drug delivery.

The *in vitro* internalization efficiency was evaluated by cellular uptake study (Figure 2B,C). CPP-modified nanoparticles (CPPD/DNA) demonstrated the highest cellular uptake efficiency, benefiting from the efficient internalization of CPP.^{28–32} Under pH 7.4, the uptake efficiency of *dtACPPD*/DNA was not ideal (34.4% relative to CPPD/DNA) even pretreated with MMP2 to cleave the linker. However, it would increase to 86.9% under pH 6.0, meaning that *dtACPP* was adequately activated to CPP to perform its internalization well in the mimetic tumor microenvironments. The result from cellular uptake of nanocarriers was similar to the nanoparticles (Supporting Information Figure S1). All of the results indicated that both MMP2 and lowered pH were indispensable in activating *dtACPP*, and this dual-triggering mechanism of *dtACPP*

made it suitable for the *in vivo* tumor-targeting application.

In vivo biodistribution and tumor-targeting characteristics of *dtACPPD*/DNA were monitored using a real-time fluorescence imaging technique. Figure 3A shows that there was a corresponding accumulation of ethidium monoazide bromide (EMA)-labeled DNA in the tumor sites 24 h after injection of respective nanoparticles, benefiting from the EPR effect.^{25–27} Meanwhile, for the *dtACPPD*/DNA-treated group, the accumulation was progressively increased and far more than both PEG-DGL/DNA- and CPPD/DNA-treated groups at 24 h (Figure 3B). There was the same tendency in that treated with the nanocarriers (Figure S2). The excised brains were sectioned to further study the *in vivo* location of nanoparticles. For the *dtACPPD*/DNA-treated group (Figure 3C,D middle column), EMA-labeled DNA accumulated highly at the boundary and interior of the tumor. Within the tumor, the overwhelming majority of the DNA accumulated in the cytoplasm and partly localized within cell nuclei, similar results previously

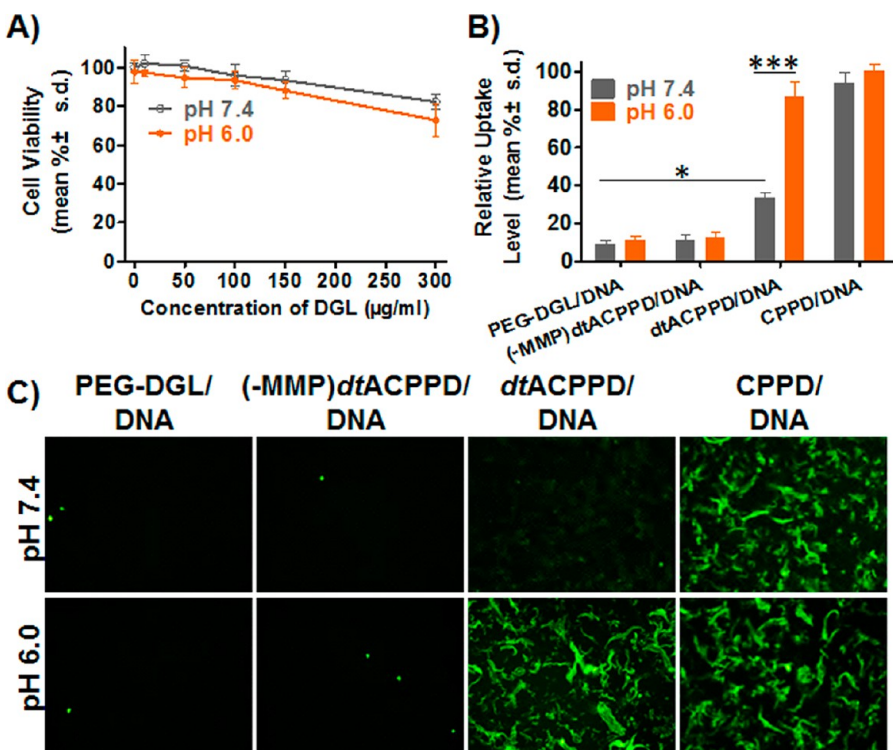


Figure 2. Toxicity and uptake efficiency of nanoparticle systems. (A) Viability of cells treated with different concentrations of *dtACPPD/DNA* under pH 7.4 or 6.0. Uptake efficiency detected by (B) flow cytometer and (C) fluorescence image of cells treated with different nanoparticles under pH 7.4 or 6.0, respectively. The geometric mean of the fluorescence for the cells treated with CPPD/DNA under pH 6.0 was defined as 100% ($n = 5$). Asterisks (*) denote statistically significant differences ($*p < 0.05$, $***p < 0.001$) calculated by one-way ANOVA test. DNA used here was prelabeled by YOYO-1, which could emit green fluorescence. Original magnification: $100\times$.

reported for polycation-mediated transduction.⁴¹ Inspiringly, the successful nuclear location is crucial to improve the expression of exogenous DNA.⁴² These results confirmed that the activation of *dtACPP* modifying on the nanoparticles mostly occurred within the tumor to internalize nanoparticles well, benefiting from the dual stimuli, lowered pH, and upregulated MMP2.⁴³ As once *dtACPP* being activated prematurely to expose CPP in the circulation, nanoparticles would accumulate too acutely in the main metabolic organs to perform the EPR effect well, just like the CPPD/DNA-treated group.

Gene Transfection. Inspired by the satisfactory tumor targetability, the *in vivo* gene transfection efficiency was evaluated after 48 h of administration, the time allowed for the uptake and expression of EGFP encoding DNA. Figure 4 indicated that *dtACPPD* could efficiently deliver intact DNA into the tumor cells for gene expressing, as evidenced by the high EGFP signal in the tumor site of the *dtACPPD/pEGFP*-treated group. The EGFP signal from the CPPD/pEGFP-treated one was obviously decreased, which might due to the non-specific distribution of CPPD/pEGFP over the whole body, especially the main metabolic organs, as shown in Figure 3. There was little EGFP signal in the one treated with PEG-DGL/pEGFP that lacked internalization efficiency. All of the results indicated that

dtACPPD/pEGFP possessed good tumor targetability and internalization efficiency once more.

Inhibition of Endogenous VEGF and Shutdown of Blood

Vessels. Real-time polymerase chain reaction (RT-PCR) was performed to evaluate the level of endogenous VEGF mRNA (Figure 5). The VEGF mRNA of *in vitro* cells was inhibited to 31.7% for *dtACPPD/shVEGF*, similar to CPPD/shVEGF (28.3%). However, the VEGF mRNA of *in vivo* glioma was inhibited to 75.5% for CPPD/shVEGF, significantly weaker than *dtACPPD/shVEGF* (34.3%). The result in the secretory VEGF protein of *in vivo* glioma was consistent with that in the mRNA level (Figure S3). The *in vitro* results indicated that the internalization and anti-VEGF efficiency of *dtACPPD/shVEGF* was close to CPPD/shVEGF in the mimetic tumor microenvironment. After systemic administration, the anti-VEGF effect of *dtACPPD/shVEGF* was obviously stronger than CPPD/shVEGF, owing to the ideal tumor targetability of the *dtACPP*-modified nanoparticles.

In addition to the investigation of endogenous VEGF, gliomas were retrieved to determine the functionality of tumor-associated blood vessels (Figure 6). Compared to other groups, *dtACPPD/shVEGF* resulted in fewer functional blood vessels and the tumor-associated blood vessels.

In Vitro Apoptosis Assay and In Vivo Apoptosis Imaging. As shown in Figure 7A,B, under the selected dose, the

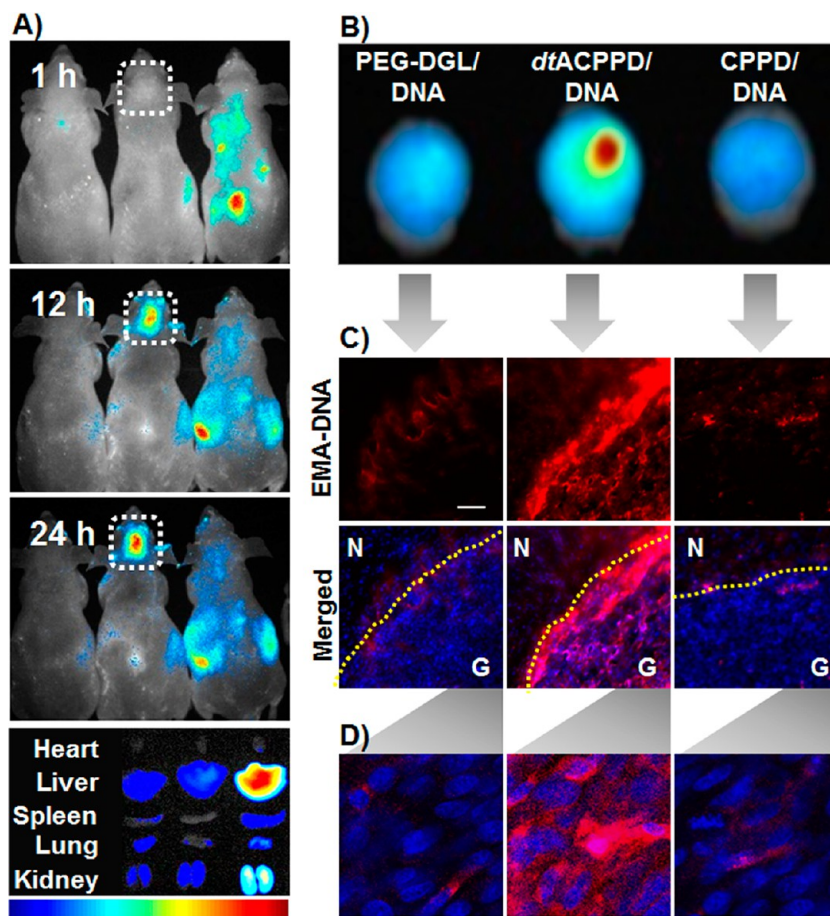


Figure 3. Real-time fluorescence imaging showed the *in vivo* distribution and subcellular location of nanoparticles in the glioma-bearing mice. (A) *In vivo* imaging of mice treated with EMA-labeled DNA that complexed with PEG-DGL (left in every image), *dt*ACPPD (middle in every image), or CPPD (right in every image). Images were taken at 1, 12, and 24 h after systemic administration. The bottom image shows the corresponding exposed main organs that were excised at 24 h after administration. (B) Imaging of the excised glioma-bearing brains. Intensity of the signal: dark red is the strongest, while dark blue is the weakest, as shown by the bar. (C) Brain sections showed the accumulation of EMA-labeled DNA at the interior of the glioma and normal brain surrounding glioma. N = normal brain; G = glioma; yellow dashed line = boundary of the glioma. Original magnification: 200 \times . (D) Corresponding subcellular localization of the DNA within the glioma. Red: EMA-labeled DNA. Blue: DAPI-stained cell nuclei.

apoptosis rate induced by *dt*ACPPD/shVEGF (7.4%) was similar to that induced by *dt*ACPPD/DNA (pGL2). This phenomenon was due to anti-VEGF therapy inhibited tumor growth *via* antiangiogenesis rather than killing off tumor cells directly. However, the apoptosis rate grew to 45.5% in the one treated with *dt*ACPPD/shVEGF–DOX, attributed to the direct and intrinsic apoptosis pathway induced by DOX.⁴⁴ It is such a delight that shVEGF might modulate the efficacy of DOX *in vivo* by normalization of tumor blood vessels.⁴⁵

Annexin-Vivo 750 was utilized to further compare the *in vivo* apoptosis efficiency induced by mono/combination therapy, which was able to bind to the apoptosis cells and reveal information about immediate cell death.⁴⁶ This *in vivo* fluorescence imaging provides convenient and rapid assessment of real-time biological processes.⁴⁷ Compared to other groups, the apoptosis within the tumor was most evident in the group treated with *dt*ACPPD/shVEGF–DOX, which might benefit from the combination efficacy of anti-VEGF therapy and chemotherapy (Figure 7C,D).⁴⁸

Just as shown in the *dt*ACPPD/shVEGF treated group, shutdown of blood vessels induced by shVEGF could starve the tumor from nutrients and oxygen, thereby reducing tumor growth and inducing extensive necrosis of tumor cells (starvation hypothesis).^{4,49} Additionally, the direct cytotoxic effects of DOX could cause cell apoptosis and decrease proliferation rate. These results renewed the hope that simultaneous targeting of blood vessels and tumor cells can improve outcomes for patients with tumors.⁴⁸

Antitumor Efficacy. Tumor histology according to TUNEL assay demonstrated that *dt*ACPPD could effectively deliver shVEGF–DOX into the tumor cells to induce tumor cell apoptosis most severely (Figure 8A).

The clinically therapeutic benefits are mainly determined based on the quality of life and prolonged survival time of cancer patients.³⁸ To further estimate the antitumor efficacy, the body weight (BW) and overall survival of the glioma-bearing mice were assessed (Figure 8B,C). The control group (saline-treated only) exhibited a rapid loss in BW and early death as a

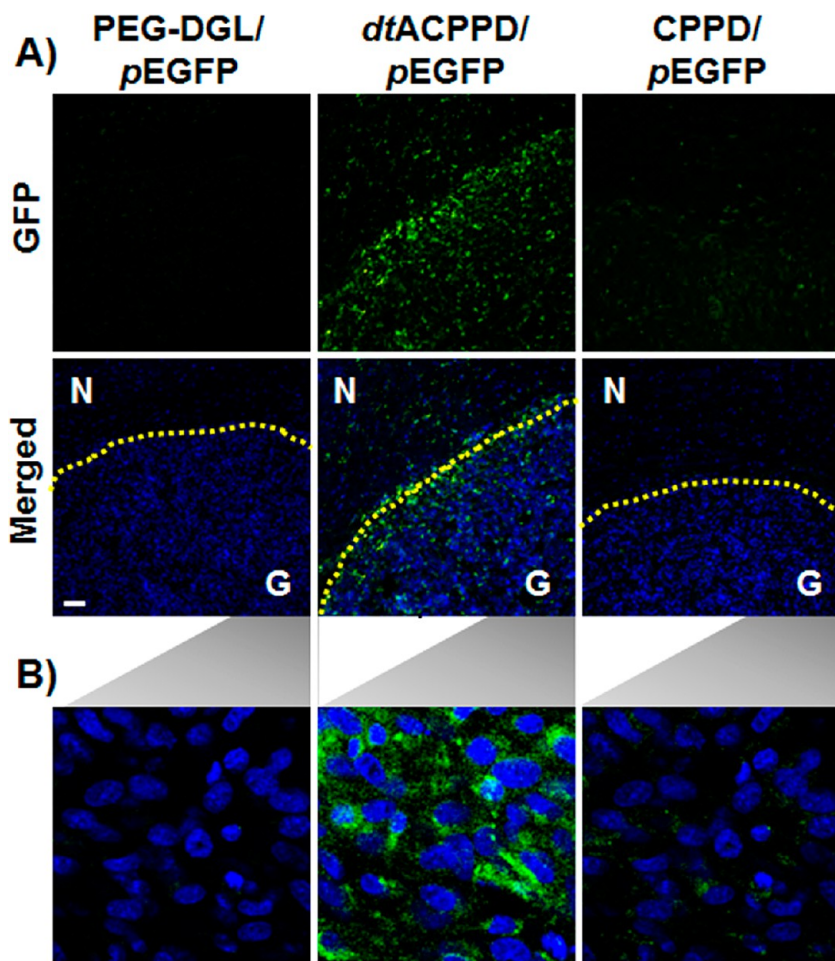


Figure 4. *In vivo* gene expression in the glioma-bearing mice. (A) Brain sections showed the gene expression at the interior of glioma and normal brain surrounding glioma. N = normal brain; G = glioma; yellow dashed line = boundary of the glioma. Scale bar: 50 μ m. (B) Gene expression within the glioma. Green: GFP. Blue: DAPI-stained cell nuclei.

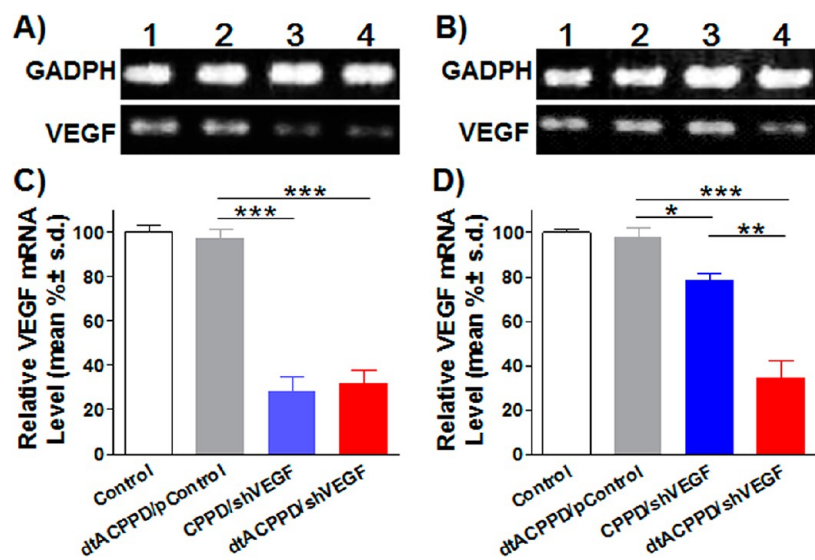


Figure 5. Inhibition of endogenous VEGF mRNA expression by transfection with shVEGF. (A,C) Representative VEGF mRNA *in vitro* and (B,D) *in vivo* was analyzed by semiquantitative RT-PCR. Lane 1, control (untreated); lane 2, *dtACPPD/pcontrol* (pGL2); lane 3, CPPD/shVEGF; lane 4, *dtACPPD/shVEGF*. GADPH was used as an internal control. (C,D) VEGF mRNA levels were quantified by RT-PCR. Data were normalized with the house-keeping gene GADPH ($n = 3$). Asterisks (*) denote statistically significant differences ($*p < 0.05$, $**p < 0.01$, $***p < 0.001$) calculated by one-way ANOVA test.

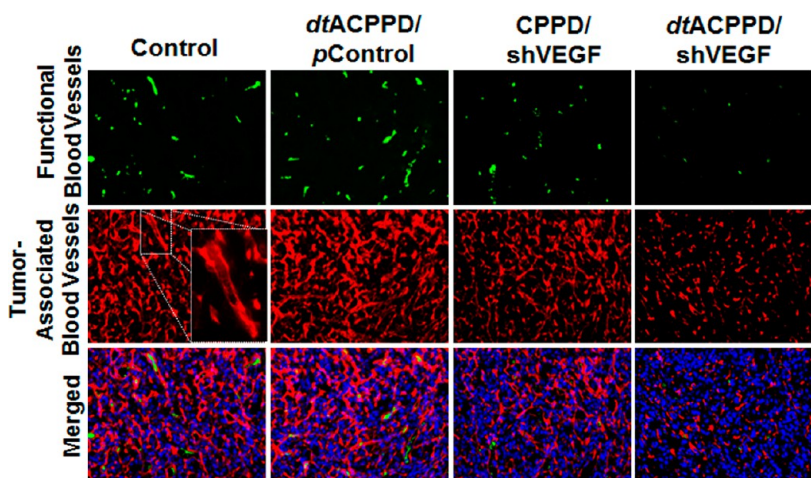


Figure 6. Blood vessels within the glioma. Functional blood vessels were detected by intravenously administrated lectin (green) while tumor-associated blood vessels (red) were stained with antibody against CD34. The cell nuclei (blue) were stained with DAPI. Original magnification: 200 \times .

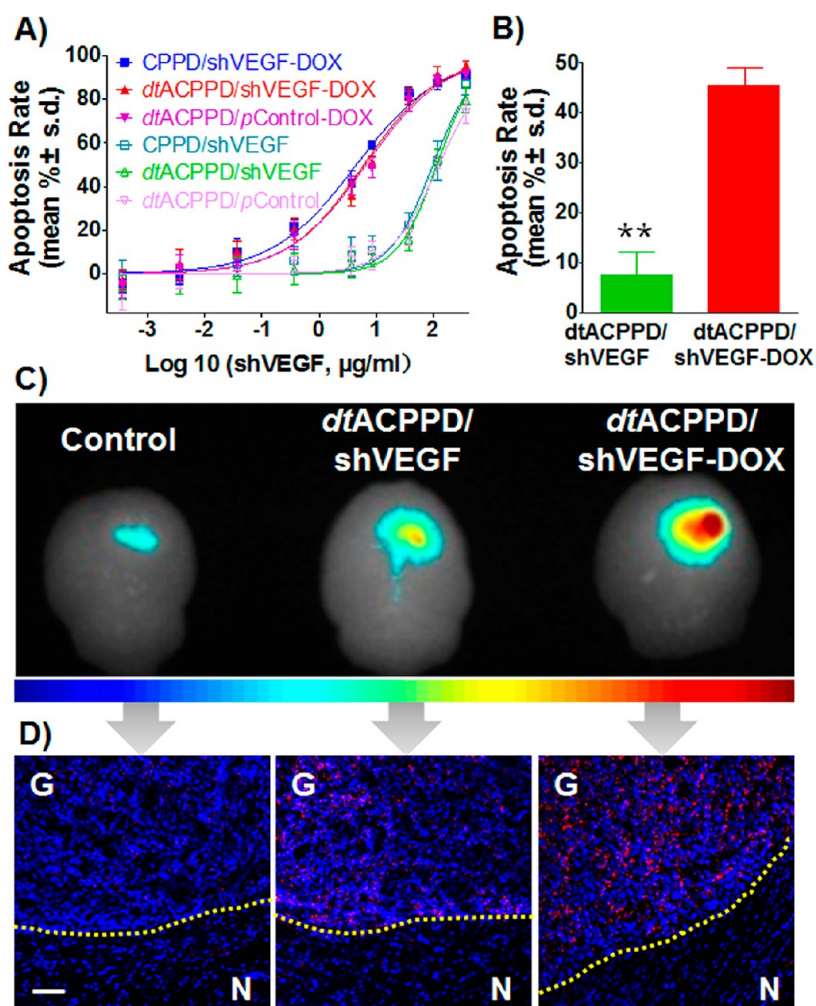


Figure 7. (A) *In vitro* apoptosis of U-87 MG cells induced by shVEGF, shVEGF-DOX, and pcontrol-DOX that was delivered with CPPD or dtACPPD ($n = 5$). (B) Comparison of apoptosis rate induced by dtACPPD/shVEGF and dtACPPD/shVEGF-DOX under the selected dose (8.33 μ g DNA (plus 1.33 μ g DOX) per mL) adopted in the *in vivo* study. Asterisks (*) denote statistically significant differences (** $p < 0.01$) calculated by one-way ANOVA test. (C) Representative *in vivo* apoptosis images 24 h after Annexin-Vivo 750 administration for different treatment groups as indicated. (D) Brain sections showed the cells' apoptosis at the interior of the glioma and normal brain surrounding glioma. N = normal brain; G = glioma; blue = DAPI-stained cell nuclei; yellow dashed line = boundary of the glioma. Scale bar: 50 μ m.

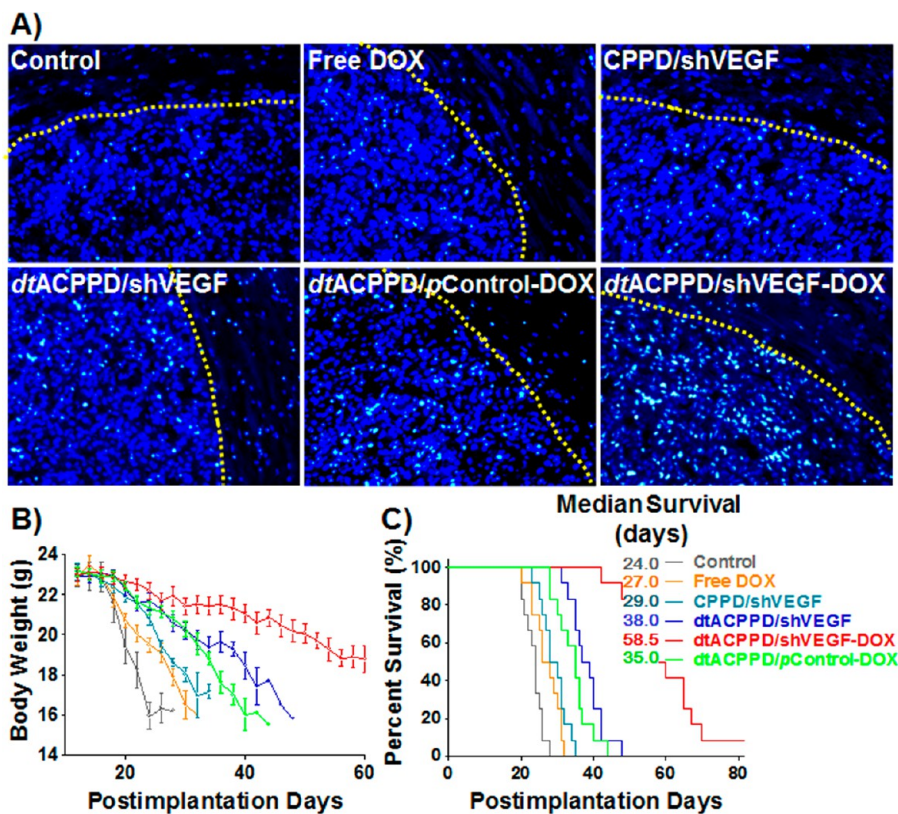


Figure 8. Antitumor efficacy. (A) Histological images of the glioma tissues using the TUNEL assay. Green: apoptosis cells. Blue: DAPI-stained cell nuclei. Yellow dashed line: boundary of the glioma. Original magnification: 200 \times . (B) Average change of body weight and (C) overall survival of glioma-bearing mice ($n = 12$).

function of time, owing to the VEGF-induced CASS. Compared with free DOX, *dtACPPD/pcontrol-DOX* possessed prolonged survival time, and the loss in BW was gentler, although their dose of DOX was self-same. In addition, *dtACPPD/shVEGF* possessed better antitumor efficacy than CPPD/shVEGF. The results once again indicated that *dtACPPD*-modified nanoparticles possessed ideal tumor-targeting function and internalization efficiency within the tumor once more. As expected, *dtACPPD/shVEGF-DOX* possessed the best antitumor efficiency, gentlest loss in BW, and the median survival time was up to 58.5 days, owing to the effective combination efficacy on the premise of effective drug delivery. The results showed that treatment with anti-VEGF agents or chemotherapeutics independently was not sufficient for oncotherapy. So it is necessary to implement the combination of antiangiogenesis and apoptosis simultaneously.¹⁶

Overall, both *in vitro* and *in vivo* results suggested that *dtACPPD*-modified nanoparticles explored in this study were an ideal platform for tumor-targeting delivery. Additionally, anti-VEGF agent, shVEGF, in

combination with DOX, exhibited an efficient antitumor efficacy. So this tumor-targeting and microenvironment-responsive nanoparticle system, *dtACPPD/shVEGF-DOX*, was an ideal candidate for antitumor therapy.

CONCLUSION

Angiogenesis, rapidly proliferating tumor cells, and tumor microenvironment are the common characteristics of most tumors, which make it practical to develop a universally valid drug delivery system. In this study, we have presented a smart and effective tumor-targeting nanoparticle system, *dtACPPD/shVEGF-DOX*, which demonstrated effective shutdown of blood vessels and cell apoptosis within the tumor. *dtACPPD/shVEGF-DOX* selectively accumulated in tumor sites via the EPR effect and further internalized into the intratumoral cells by the exposed CPP, which was activated in the unique tumor microenvironment. On the premise of effective drug delivery, the combination therapy of antiangiogenesis and apoptosis has achieved ideal antitumor efficacy that obviously prolonged the survival time of glioma-bearing mice.

MATERIALS AND METHODS

Materials. DGL G3 dendrimer with 123 lysine groups was purchased from Colcom, France. α -Maleimidyl- ω -N-hydroxysuccinimidyl

polyethyleneglycol (MAL-PEG-NHS, MW 3500) was purchased from Jenkem Technology Co., Ltd. (Beijing, China). Peptides e₄k₄-x-PLLAG-r₉-x-c (*dtACPP*, MMP2 cleavable peptide) and

r_9 -x- c (CPP, positive control) were synthesized by Chinese Peptide Company (Hangzhou, China). Lowercase letters indicated α -amino acids, and x is an aminohexanoic linker. Recombinant-human MMP2 proenzyme was obtained from EMD. YOYO-1 iodide, ethidium monoazide bromide (EMA), and 4,6-diamidino-2-phenylindole (DAPI) were purchased from Molecular Probes (Eugene, OR, USA). The plasmid pGL2, pEGFP-N2, and shVEGF (Clontech, Palo Alto, CA, USA) were purified using QIAGEN Plasmid Mega kit (Qiagen GmbH, Hilden, Germany).

Nanocarrier Synthesis. DGL was reacted with PEG at the ratio 1:10 (mol/mol) in PBS (pH 8.0) for 2 h at room temperature. The resulting conjugate, PEG-DGL, was purified by ultrafiltration through a membrane (cutoff = 5 kDa) and dissolved in PBS (pH 7.0). Then PEG-DGL was reacted with *dtACPPD* at the ratio of 1:5 (DGL to peptide, mol/mol) in PBS (pH 7.0) for 24 h at room temperature. The MAL groups of PEG were specifically reacted with the thiol groups of *dtACPPD* to form the corresponding nanocarrier, *dtACPPD*.

1H NMR. The characteristic of *dtACPPD* was analyzed by 1H NMR spectroscopy. Basically, DGL, PEG-DGL, and *dtACPPD* were purified by ultrafiltration through a membrane (cutoff = 5 kDa), then freeze-dried, solubilized in D_2O , and analyzed on a 400 MHz spectrometer (Varian, Palo Alto, CA, USA).

Monitoring of DNA–DOX Complex Formation by Fluorescence. A physical complex between shVEGF and DOX was made as described previously.¹⁸ Briefly, different concentrations of plasmid in a fixed volume (500 μ L) were added to a fixed concentration of DOX (6 μ M, 500 μ L) in PBS buffer; the mixture was vortexed for 1 min, and the fluorescence of DOX was monitored at an excitation of 480 nm and emission recorded in the interval of 520–680 nm (1.5 mm slit) on a Perkin-Elmer LS-55 spectrofluorometer.

Preparation of Nanoparticles. The freshly prepared nanocarrier was diluted to appropriate concentration, and then the DNA or DNA–DOX solution (100 μ g DNA/mL in 50 mM sodium sulfate solution) was added to obtain specified weight ratio and immediately vortexed for 30 s. Freshly prepared nanoparticles were used in the following experiments. In the evaluation of *in vivo* distribution, the DNA was labeled with EMA, the fluorescent photoaffinity label. DNA solution (1 mg/mL in TE buffer, pH 7.0) was diluted to 0.1 mg/mL with an aqueous solution of EMA (1 mg/mL) and incubated for 30 min away from light at room temperature. The complex was then exposed to UV light (365 nm) for 1 h, and the resulting solution was precipitated by adding ethanol to a final concentration of 30% (v/v). The precipitate was collected by centrifugation and redissolved in 50 mM sodium sulfate solution.

Gel Retardation Assays. Agarose gel retardation assay was carried out to determine the DNA–DOX binding ability of *dtACPPD*. *dtACPPD*/DNA–DOX was prepared at various weight ratios (DGL to DNA; 0.1:1, 0.5:1, 1:1, 2:1, 4:1, 6:1, and 8:1). The complexes were mixed with appropriate amounts of 6 \times loading buffer and then electrophoresed on a 0.9% (w/v) agarose gel containing ethidium bromide (0.25 μ g/mL of the gel). The location of DNA in the gel was analyzed on a UV illuminator and photographed using a Canon IXUS 950IS camera.

Characterization of *dtACPPD*/DNA–DOX. The mean diameter and zeta-potential of *dtACPPD*/DNA–DOX with a DGL to DNA weight ratio at 6:1 under pH 7.4 or 6.0 were determined by a Zetasizer Nano (Marvin Instruments Ltd., UK). Also, their morphology was examined under atomic force microscopy (Veeco Instruments, USA).

Pretreatment of MMP2. It has been demonstrated that, although the tumor cells secret MMP2, the enzyme becomes notably diluted in *in vitro* experiment, resulting in slow cleavage and negligible activation. In addition, it has been found that significant cleavage and uptake of ACPPs required pre-cleavage with exogenous protease.^{31,32} Recombinant-human MMP2 proenzyme (5 μ g in 80 μ L of 50 mM Tris-HCl buffer) was activated with 2.5 mM 4-aminophenylmercuric acetate at 37 °C for 2 h. Before cell incubation, *dtACPPD* was activated with MMP2 (10 pmol) for 3 h in 50 mM Tris, 200 mM NaCl, 10 mM $CaCl_2$, and 10 μ M $ZnCl_2$ under pH 7.5. *dtACPPD* without pretreatment of MMP2 was designated as (–MMP)*dtACPPD*.

Evaluation of Cytotoxicity Induced by *dtACPPD*. The toxicity induced by the nanocarrier, *dtACPPD*, was evaluated by *dtACPPD*/DNA (pGL2, negative control plasmid) in U-87 MG cells, via (3-(4,5-dimethylthiazol-2-yl)-2,5-diphenyltetrazolium bromide (MTT) assay. U-87 MG cells were seeded in 96-well culture plates (Corning-Coaster, Tokyo, Japan) at a density of 5000 cells/well. When achieving 70–80% confluence, the cells were incubated with *dtACPPD*/DNA solutions with various concentrations at 40 μ L/well of the serum-free medium under pH 7.4 or 6.0. After 60 min incubation, MTT assay was performed. Cell viability of each group was expressed as a percentage relative to that of untreated control.

Cellular Uptake. U-87 MG cells were seeded in 24-well culture plates (Corning-Coaster, Tokyo, Japan) at a density of 3×10^4 cells/well. When achieving 70–80% confluence, the cells were incubated with the DNA (pGL2) complexed with various nanocarrier systems (PEG-DGL, (–MMP)*dtACPPD*, *dtACPPD*, or CPPD) at the concentration of 10 μ g DGL in 200 μ L/well of the serum-free medium under pH 7.4 or 6.0. After 30 min incubation, the medium was removed, and the cells were washed with PBS three times and then visualized and photographed under an IX2-RFACA fluorescent microscope (Olympus, Osaka, Japan). DNA used here was prelabeled by YOYO-1, which could intercalate into DNA and emit green fluorescence. For flow cytometry, the cells were seeded in 6-well culture plates (Corning-Coaster, Tokyo, Japan) at a density of 1×10^5 cells/well. The following incubating operation was the same as the former. After that, the cells were trypsinized and collected by centrifugation at 1200 rpm for 5 min. After washing with ice-cold PBS, the cell pellet was resuspended in 100 μ L of PBS and applied immediately on a FACS Calibur flow cytometer (Epics Altra, USA).

Tumor Implantation. All animal experiments were carried out in accordance with guidelines evaluated and approved by the ethics committee of Fudan University, Shanghai, China. Glioma-bearing mice were prepared by intracranial injection (striatum, 1.8 mm right lateral to the bregma and 3 mm of depth) of 1×10^5 U-87 MG cells suspended in serum-free media into male nude mice with body weight of 20–25 g (Sino-British Sippr/BK Lab. Animal Ltd.).

In Vivo Distribution and Gene Transfection. At the 18th day after implantation, glioma-bearing mice were injected intravenously through the tail vein with 200 μ L of PEG-DGL/DNA, *dtACPPD*/DNA, or CPPD/DNA (6:1, DGL to DNA, w/w) at a dose of 50 μ g DNA, respectively. Then, 1, 12, and 24 h after administration, the mice were anesthetized and visualized by a Cambridge Research & Instrumentation *in vivo* imaging system (CRI, MA, USA). After that, mice were sacrificed and the glioma-bearing brains and other main organs (heart, liver, spleen, lung, and kidneys) were excised carefully to compare the relative accumulation. DNA used here was prelabeled by EMA which could intercalate into DNA and emit red fluorescence. After dehydration, glioma-bearing brains were frozen in OCT embedding medium (Sakura, Torrance, CA, USA). Frozen sections of 20 μ m thickness were prepared with a cryotome Cryostat (Leica, CM 1900, Wetzlar, Germany) and stained with 300 nM DAPI for 10 min at room temperature. After washing twice with PBS, the sections were immediately examined under the IX2-RFACA fluorescent microscope (Olympus, Osaka, Japan) and confocal laser scanning microscope (Olympus, Fluoview FV100, Japan). For the *in vivo* gene expression, nanoparticles containing pEGFP-N2 were injected into the tail vein of glioma-bearing mice at a dose of 50 μ g DNA/mouse. Forty-eight hours later, mice were anesthetized and the subsequent section and observation operation was the same as above.

Vascular Detection. To detect the vascular function and density within the glioma, 100 μ L of biotinylated tomato lectin (10 μ g/mL in PBS, from Vector Laboratories, Burlingame, CA) was injected intravenously 1 h prior to the animal sacrifice.⁵⁰ The excised glioma-bearing brains were sectioned for antibody and DAPI staining. Tumor-associated blood vessels were detected with rhodamine-labeled anti-CD34 antibody (Vector Laboratories) labeled by Alexa Fluor 555, while the functional vessels that had been stained with the biotinylated lectin were detected with a streptavidin-conjugated Alexa Fluor 488 (Invitrogen).

RT-PCR for Evaluating VEGF mRNA. U-87 MG cells were seeded in 6-well culture plates at a density of 2×10^5 cells/well. Forty-eight hours later, the cells were incubated with *dtACPPD/pcontrol* (pGL2), CPPD/shVEGF, and *dtACPPD/shVEGF* (6:1, DGL to DNA, w/w) at the concentration of 8.33 μg DNA/mL (500 μL /well) with serum-free medium under pH 6.0. The cells that were only treated with serum-free medium under pH 6.0 were designed as control. After 30 min incubation, the medium was removed, and the cells were washed with PBS three times. After that, the cells were further incubated in the fresh medium. After continuous culture for 48 h, the cells were collected for total RNA extraction. At the 12th, 15th, and 18th day after implantation, *dtACPPD/pcontrol* (pGL2), CPPD/shVEGF, and *dtACPPD/shVEGF* (6:1, DGL to DNA, w/w) at the dose of 50 μg DNA/mouse were injected into the tail vein of glioma-bearing mice, respectively. At day 21, the glioma tissues were excised for extraction of total RNA and protein. *In vitro* and *in vivo* expression of VRGF mRNA was detected by semiquantitative RT-PCR. Total RNA was extracted by using TRIzol reagent, and possible DNA contamination was removed by digesting the extracted RNA with DNase I (Invitrogen). The RNA was purified again using TRIzol reagent and subjected to the synthesis of first-strand cDNA using a reverse transcription kit (Invitrogen). GADPH was amplified as an internal control. The sequence of the VEGF forward primer was 5'-GGCAGAATCATCACGAACTGGTG-3', and reverse primer was 5'-GGGTCTCGATTGGATGGCAGTAG-3'. All primers were synthesized by GenePharma Co., Ltd. (Shanghai, China).

Cell Apoptosis Assay. U-87 MG cells were seeded in 96-well culture plates at a density of 5000 cells/well. When achieving 70–80% confluence, the cells were incubated with various doses of CPPD/shVEGF, *dtCPPD/shVEGF*, *dtCPPD/pcontrol* (pGL2), CPPD/shVEGF–DOX, *dtCPPD/shVEGF*–DOX, or *dtCPPD/pcontrol*–DOX at 37 °C in the serum-free medium under pH 6.0. After 30 min incubation, the medium was removed and the cells were washed with PBS three times. After that, the cells were further incubated in the fresh medium. Forty-eight hours later, MTT assay was performed.

In Vivo Pharmacodynamic Evaluation and Survival Monitoring. The glioma-bearing mice were randomized to six groups (15 mice/group). At the 12th, 15th, and 18th day after the implantation, each group of mice was treated with intravenously administration of CPPD/shVEGF, *dtACPPD/shVEGF*, *dtACPPD/shVEGF*–DOX, and *dtACPPD/pcontrol*–DOX (pGL2) at a dose of 50 μg DNA (plus 8 μg DOX) per mouse. For free DOX, mice were intravenously injected with 8 μg DOX/mouse. The saline-treated group was used as control. There were 12 mice/group monitored for body weight change and overall survival, and others were used for the following experiment at day 21. For *in vivo* apoptotic imaging, the mice that had been treated with saline, *dtACPPD/shVEGF*, or *dtACPPD/shVEGF*–DOX received 100 μL /mouse of apoptotic agent Annexin-Vivo (excited at 740 nm; emission collected at 780 nm). Imaging was conducted at 24 h post-annexin administration by a CRi *in vivo* imaging system. Enhancement in signal intensity can be attributed to an increase in annexin binding at the tumor site. After that, mice were sacrificed and the glioma-bearing brains were sectioned, stained with DAPI, and examined under the IX2-RFACA fluorescent microscope (Olympus, Osaka, Japan). For the broken nuclear DNA fragment detection, the glioma-bearing brains from all groups were frozen sectioned, subjected to terminal deoxynucleotidyl transferase-mediated nick end labeling (TUNEL) to detect the broken nuclear DNA fragments, stained with DAPI, and examined under the IX2-RFACA fluorescent microscope (Olympus, Osaka, Japan).

Conflict of Interest: The authors declare no competing financial interest.

Acknowledgment. This work was supported by the grant from National Basic Research Program of China (973 Program, 2013CB932500), National Natural Science Foundation of China (81172993), and Program for New Century Excellent Talents in University.

Supporting Information Available: Cellular uptake of nanocarriers, *in vivo* imaging of nanocarrier-treated groups, and Western blotting. This material is available free of charge via the Internet at <http://pubs.acs.org>.

REFERENCES AND NOTES

- Chambers, A. F.; Groom, A. C.; MacDonald, I. C. Dissemination and Growth of Cancer Cells in Metastatic Sites. *Nat. Rev. Cancer* **2002**, *2*, 563–572.
- Folkman, J. What Is the Evidence That Tumors Are Angiogenesis Dependent. *J. Natl. Cancer Inst.* **1990**, *82*, 4–6.
- McMahon, G. VEGF Receptor Signaling in Tumor Angiogenesis. *Oncologist* **2000**, *5*, 3–10.
- Jain, R. K.; di Tomaso, E.; Duda, D. G.; Loeffler, J. S.; Sorensen, A. G.; Batchelor, T. T. Angiogenesis in Brain Tumours. *Nat. Rev. Neurosci.* **2007**, *8*, 610–622.
- Ohta, Y.; Endo, Y.; Tanaka, M.; Shimizu, J.; Oda, M.; Hayashi, Y.; Watanabe, Y.; Sasaki, T. Significance of Vascular Endothelial Growth Factor Messenger RNA Expression in Primary Lung Cancer. *Clin. Cancer Res.* **1996**, *2*, 1411–1416.
- Liu, T.; Ye, L.; He, Y.; Chen, X.; Peng, J.; Zhang, X.; Yi, H.; Peng, F.; Leng, A. Combination Gene Therapy Using VEGF-shRNA and Fusion Suicide Gene yCDglyTK Inhibits Gastric Carcinoma Growth. *Exp. Mol. Pathol.* **2011**, *91*, 745–752.
- Xue, Y.; Religa, P.; Cao, R.; Hansen, A. J.; Lucchini, F.; Jones, B.; Wu, Y.; Zhu, Z.; Pytowski, B.; Liang, Y.; et al. Anti-VEGF Agents Confer Survival Advantages to Tumor-Bearing Mice by Improving Cancer-Associated Systemic Syndrome. *Proc. Natl. Acad. Sci. U.S.A.* **2008**, *105*, 18513–18518.
- Reardon, D. A.; Wen, P. Y.; Desjardins, A.; Batchelor, T. T.; Vredenburgh, J. J. Glioblastoma Multiforme: An Emerging Paradigm of Anti-VEGF Therapy. *Expert Opin. Biol. Ther.* **2008**, *8*, 541–553.
- Miletic, H.; Niclou, S. P.; Johansson, M.; Bjerkvig, R. Anti-VEGF Therapies for Malignant Glioma: Treatment Effects and Escape Mechanisms. *Expert Opin. Ther. Targets* **2009**, *13*, 455–468.
- Wick, W.; Weller, M.; van den Bent, M.; Stupp, R. Bevacizumab and Recurrent Malignant Gliomas: A European Perspective. *J. Clin. Oncol.* **2010**, *28*, 188–189.
- Aagaard, L.; Rossi, J. J. RNAi Therapeutics: Principles, Prospects and Challenges. *Adv. Drug Delivery Rev.* **2007**, *59*, 75–86.
- Hu, Q.; Li, W.; Hu, X.; Hu, Q.; Shen, J.; Jin, X.; Zhou, J.; Tang, G.; Chu, P. K. Synergistic Treatment of Ovarian Cancer by Co-delivery of Survivin shRNA and Paclitaxel via Supramolecular Micellar Assembly. *Biomaterials* **2012**, *33*, 6580–6591.
- Guan, H.; Zhou, Z.; Wang, H.; Jia, S. F.; Liu, W.; Kleinerman, E. S. A Small Interfering RNA Targeting Vascular Endothelial Growth Factor Inhibits Ewing's Sarcoma Growth in a Xenograft Mouse Model. *Clin. Cancer Res.* **2005**, *11*, 2662–2669.
- Detwiller, K. Y.; Fernando, N. T.; Segal, N. H.; Ryeom, S. W.; D'Amore, P. A.; Yoon, S. S. Analysis of Hypoxia-Related Gene Expression in Sarcomas and Effect of Hypoxia on RNA Interference of Vascular Endothelial Cell Growth Factor A. *Cancer Res.* **2005**, *65*, 5881–5889.
- Salva, E.; Kabasakal, L.; Eren, F.; Cakalagaoglu, F.; Ozkan, N.; Akbuga, J. Chitosan/Short Hairpin RNA Complexes for Vascular Endothelial Growth Factor Suppression Invasive Breast Carcinoma. *Oligonucleotides* **2010**, *20*, 183–190.
- Ren, B.; Song, K.; Parangi, S.; Jin, T.; Ye, M.; Humphreys, R.; Duquette, M.; Zhang, X.; Benhaga, N.; Lawler, J.; et al. A Double Hit To Kill Tumor and Endothelial Cells by TRAIL and Antiangiogenic 3TSR. *Cancer Res.* **2009**, *69*, 3856–3865.
- Zhu, C.; Jung, S.; Luo, S.; Meng, F.; Zhu, X.; Park, T. G.; Zhong, Z. Co-delivery of siRNA and Paclitaxel into Cancer Cells by Biodegradable Cationic Micelles Based on PDMAEMA-PCL-PDMAEMA Triblock Copolymers. *Biomaterials* **2010**, *31*, 2408–2416.
- Bagalkot, V.; Lee, I. H.; Yu, M. K.; Lee, E.; Park, S.; Lee, J. H.; Jon, S. A Combined Chemoimmunotherapy Approach Using a Plasmid–Doxorubicin Complex. *Mol. Pharmaceutics* **2009**, *6*, 1019–1028.
- Bagalkot, V.; Farokhzad, O. C.; Langer, R.; Jon, S. An Aptamer-Doxorubicin Physical Conjugate as a Novel Targeted Drug-Delivery Platform. *Angew. Chem., Int. Ed.* **2006**, *45*, 8149–8152.

20. Guo, L.; Fan, L.; Pang, Z.; Ren, J.; Ren, Y.; Li, J.; Chen, J.; Wen, Z.; Jiang, X. TRAIL and Doxorubicin Combination Enhances Anti-glioblastoma Effect Based on Passive Tumor Targeting of Liposomes. *J. Controlled Release* **2011**, *154*, 93–102.
21. Han, L.; Huang, R.; Li, J.; Liu, S.; Huang, S.; Jiang, C. Plasmid pORF-hTRAIL and Doxorubicin Co-delivery Targeting to Tumor Using Peptide-Conjugated Polyamidoamine Dendrimer. *Biomaterials* **2011**, *32*, 1242–1252.
22. Schwartz, S. M.; Heimark, R. L.; Majesky, M. W. Developmental Mechanisms Underlying Pathology of Arteries. *Physiol. Rev.* **1990**, *70*, 1177–1209.
23. Klagsbrun, M. Regulators of Angiogenesis: Stimulators, Inhibitors, and Extracellular Matrix. *J. Cell. Biochem.* **1991**, *47*, 199–200.
24. Pisters, P. W.; Patel, S. R.; Prieto, V. G.; Thall, P. F.; Lewis, V. O.; Feig, B. W.; Hunt, K. K.; Yasko, A. W.; Lin, P. P.; Jacobson, M. G.; et al. Phase I Trial of Preoperative Doxorubicin-Based Concurrent Chemoradiation and Surgical Resection for Localized Extremity and Body Wall Soft Tissue Sarcomas. *J. Clin. Oncol.* **2004**, *22*, 3375–3380.
25. Bartlett, D. W.; Su, H.; Hildebrandt, I. J.; Weber, W. A.; Davis, M. E. Impact of Tumor-Specific Targeting on the Biodistribution and Efficacy of siRNA Nanoparticles Measured by Multimodality *In Vivo* Imaging. *Proc. Natl. Acad. Sci. U.S.A.* **2007**, *104*, 15549–15554.
26. Torchilin, V. Tumor Delivery of Macromolecular Drugs Based on the EPR Effect. *Adv. Drug Delivery Rev.* **2011**, *63*, 131–135.
27. Matsumura, Y.; Oda, T.; Maeda, H. General Mechanism of Intratumor Accumulation of Macromolecules: Advantage of Macromolecular Therapeutics. *Gan to Kagaku Ryoho* **1987**, *14*, 821–829.
28. Vives, E.; Schmidt, J.; Pelegrin, A. Cell-Penetrating and Cell-Targeting Peptides in Drug Delivery. *Biochim. Biophys. Acta* **2008**, *1786*, 126–138.
29. Vives, E. Present and Future of Cell-Penetrating Peptide Mediated Delivery Systems: “Is the Trojan Horse Too Wild To Go Only to Troy?”. *J. Controlled Release* **2005**, *109*, 77–85.
30. Heitz, F.; Morris, M. C.; Divilta, G. Twenty Years of Cell-Penetrating Peptides: From Molecular Mechanisms to Therapeutics. *Br. J. Pharmacol.* **2009**, *157*, 195–206.
31. Aguilera, T. A.; Olson, E. S.; Timmers, M. M.; Jiang, T.; Tsien, R. Y. Systemic *In Vivo* Distribution of Activatable Cell Penetrating Peptides Is Superior to That of Cell Penetrating Peptides. *Integr. Biol.* **2009**, *1*, 371–381.
32. Jiang, T.; Olson, E. S.; Nguyen, Q. T.; Roy, M.; Jennings, P. A.; Tsien, R. Y. Tumor Imaging by Means of Proteolytic Activation of Cell-Penetrating Peptides. *Proc. Natl. Acad. Sci. U.S.A.* **2004**, *101*, 17867–17872.
33. Lee, E. S.; Gao, Z.; Bae, Y. H. Recent Progress in Tumor pH Targeting Nanotechnology. *J. Controlled Release* **2008**, *132*, 164–170.
34. Egeblad, M.; Werb, Z. New Functions for the Matrix Metalloproteinases in Cancer Progression. *Nat. Rev. Cancer* **2002**, *2*, 161–174.
35. Cottet, H.; Martin, M.; Papillaud, A.; Souaid, E.; Collet, H.; Commeyras, A. Determination of Dendrigraft Poly-L-lysine Diffusion Coefficients by Taylor Dispersion Analysis. *Biomacromolecules* **2007**, *8*, 3235–3243.
36. Huang, R.; Liu, S.; Shao, K.; Han, L.; Ke, W.; Liu, Y.; Li, J.; Huang, S.; Jiang, C. Evaluation and Mechanism Studies of PEGylated Dendrigraft Poly-L-Lysines as Novel Gene Delivery Vectors. *Nanotechnology* **2010**, *21*, 265101.
37. de Vries, N. A.; Beijnen, J. H.; Boogerd, W.; van Tellingen, O. Blood-Brain Barrier and Chemotherapeutic Treatment of Brain Tumors. *Expert Rev. Neurother.* **2006**, *6*, 1199–1209.
38. Friedman, H. S.; Prados, M. D.; Wen, P. Y.; Mikkelsen, T.; Schiff, D.; Abrey, L. E.; Yung, W. K.; Paleologos, N.; Nicholas, M. K.; Jensen, R.; et al. Bevacizumab Alone and in Combination with Irinotecan in Recurrent Glioblastoma. *J. Clin. Oncol.* **2009**, *27*, 4733–4740.
39. Clark, M. J.; Homer, N.; O'Connor, B. D.; Chen, Z.; Eskin, A.; Lee, H.; Merriman, B.; Nelson, S. F. U87MG Decoded: The Genomic Sequence of a Cytogenetically Aberrant Human Cancer Cell Line. *PLoS Genet.* **2010**, *6*, e1000832.
40. Im, S. A.; Gomez-Manzano, C.; Fueyo, J.; Liu, T. J.; Ke, L. D.; Kim, J. S.; Lee, H. Y.; Steck, P. A.; Kyritsis, A. P.; Yung, W. K. Antiangiogenesis Treatment for Gliomas: Transfer of Anti-sense-Vascular Endothelial Growth Factor Inhibits Tumor Growth *in vivo*. *Cancer Res.* **1999**, *59*, 895–900.
41. Potocky, T. B.; Menon, A. K.; Gellman, S. H. Cytoplasmic and Nuclear Delivery of a TAT-Derived Peptide and a β -Peptide after Endocytic Uptake into HeLa Cells. *J. Biol. Chem.* **2003**, *278*, 50188–50194.
42. Pouton, C. W.; Seymour, L. W. Key Issues in Non-viral Gene Delivery. *Adv. Drug Delivery Rev.* **2001**, *46*, 187–203.
43. Jiang, T.; Olson, E. S.; Nguyen, Q. T.; Roy, M.; Jennings, P. A.; Tsien, R. Y. Tumor Imaging by Means of Proteolytic Activation of Cell-Penetrating Peptides. *Proc. Natl. Acad. Sci. U.S.A.* **2004**, *101*, 17867–17872.
44. Danial, N. N.; Korsmeyer, S. J. Cell Death: Critical Control Points. *Cell* **2004**, *116*, 205–219.
45. Jain, R. K. Normalization of Tumor Vasculature: An Emerging Concept in Antiangiogenic Therapy. *Science* **2005**, *307*, 58–62.
46. Schutters, K.; Reutelingsperger, C. Phosphatidylserine Targeting for Diagnosis and Treatment of Human Diseases. *Apoptosis* **2010**, *15*, 1072–1082.
47. Ghoroghchian, P. P.; Therien, M. J.; Hammer, D. A. *In Vivo* Fluorescence Imaging: A Personal Perspective. *Wiley Interdiscip. Rev. Nanomed. Nanobiotechnol.* **2009**, *1*, 156–167.
48. Vredenburgh, J. J.; Desjardins, A.; Herndon, J. E., II; Dowell, J. M.; Reardon, D. A.; Quinn, J. A.; Rich, J. N.; Sathornsumetee, S.; Gururangan, S.; Wagner, M.; et al. Phase II Trial of Bevacizumab and Irinotecan in Recurrent Malignant Glioma. *Clin. Cancer Res.* **2007**, *13*, 1253–1259.
49. Bisacchi, D.; Benelli, R.; Vanzetto, C.; Ferrari, N.; Tosetti, F.; Albini, A. Anti-angiogenesis and Angioprevention: Mechanisms, Problems and Perspectives. *Cancer Detect. Prev.* **2003**, *27*, 229–238.
50. Thurston, G.; McLean, J. W.; Rizen, M.; Baluk, P.; Haskell, A.; Murphy, T. J.; Hanahan, D.; McDonald, D. M. Cationic Liposomes Target Angiogenic Endothelial Cells in Tumors and Chronic Inflammation in Mice. *J. Clin. Invest.* **1998**, *101*, 1401–1413.